DOI: 10.1534/genetics.106.063115

SWAN-1, a *Caenorhabditis elegans* WD Repeat Protein of the AN11 Family, Is a Negative Regulator of Rac GTPase Function

Yieyie Yang,*[,1] Jiamiao Lu,* Joel Rovnak,[†] Sandra L. Quackenbush[†] and Erik A. Lundquist*[,2]

**Department of Molecular Biosciences, University of Kansas, Lawrence, Kansas 66045 and [†]Department of Microbiology, Immunology and Pathology, College of Veterinary Medicine and Biomedical Sciences, Colorado State University, Fort Collins, Colorado 80523-1619*

Manuscript received July 7, 2006
Accepted for publication September 3, 2006

ABSTRACT

Rac GTPases are key regulators of cell shape and cytoskeletal organization. While some regulators of Rac activity are known, such as GTPase-activating proteins (GAPs) that repress Rac activity, other Rac regulators remain to be identified. The novel *Caenorhabditis elegans* WD-repeat protein SWAN-1 was identified in a yeast two-hybrid screen with the LIM domains of the Rac effector UNC-115/abLIM. SWAN-1 was found to also associate physically with Rac GTPases. The *swan-1(ok267)* loss-of-function mutation suppressed defects caused by the hypomorphic *ced-10(n1993)* allele and enhanced ectopic lamellipodia and filopodia formation induced by constitutively active Rac in *C. elegans* neurons. Furthermore, SWAN-1(+) transgenic expression suppressed the effects of overactive Rac, including ectopic lamellipodia and filopodia formation in *C. elegans* neurons, ectopic lamellipodia formation in cultured mammalian fibroblasts, and cell polarity and actin cytoskeleton defects in yeast. These studies indicate that SWAN-1 is an inhibitor of Rac GTPase function in cellular morphogenesis and cytoskeletal organization. While broadly conserved across species, SWAN-1 family members show no sequence similarity to previously known Rac inhibitors.

CELL and growth cone migration and the establishment and maintenance of cell shape are tightly regulated processes controlled by extracellular cues and intracellular physiology (Tessier-Lavigne and Goodman 1996; Yu and Bargmann 2001; Dickson 2002; Raftopoulou and Hall 2004; Vicente-Manzanares *et al.* 2005). Rac GTPases of the Rho subfamily are key regulators of cell shape and act in part by controlling the structure and dynamics of the actin cytoskeleton (Hall 1998). Classically, Rac GTPases were identified by their similarity to Rho and were found to induce the formation of veil-like lamellipodial plasma membrane extensions in serum-starved fibroblasts (Hall 1998; Otieno *et al.* 2005). In *Caenorhabditis elegans* neurons, Rac activity promotes the formation of both lamellipodia and filopodia, thin finger-like plasma membrane extensions (Struckhoff and Lundquist 2003). Loss-of-function studies in Drosophila and *C. elegans* demonstrate that Rac GTPases are required for a wide variety of morphogenetic events, including axon pathfinding and cell migration (Dickson 2001; Lundquist 2003). The GTPase regulatory cycle involves active, GTP-bound Racs that hydrolyze GTP to GDP and thus self-inactivate, as the GDP-bound form is inactive. Guanine nucleotide exchange factors (GEFs) mediate the exchange of GDP for GTP and thus favor the GTP-bound active state of Racs. GTPase-activating proteins (GAPs) stimulate the GTPase activity of Racs and thus favor the inactive state (Van Aelst and D'Souza-Schorey 1997). Another class of Rho GTPase negative regulators are the guanine nucleotide dissociation inhibitors (GDIs), which inhibit Rho GTPase association with the plasma membrane where they are active (Van Aelst and D'Souza-Schorey 1997; Michaelson *et al.* 2001).

In *C. elegans*, three Rac GTPases (CED-10, MIG-2, and RAC-2) have compensatory, redundant roles in axon pathfinding and in the migration of neurons, embryonic cells during gastrulation, and vulval cells (Lundquist *et al.* 2001; Kishore and Sundaram 2002; Soto *et al.* 2002). The actin-binding protein UNC-115/abLIM, which acts with Racs in axon pathfinding, is required for Rac-induced lamellipodia and filopodia in neurons and UNC-115 itself induces the formation of lamellipodia and filopodia in *C. elegans* neurons and in serum-starved mammalian fibroblasts (Lundquist *et al.* 1998; Struckhoff and Lundquist 2003; Yang and Lundquist 2005). UNC-115 might be a downstream cytoskeletal effector of Rac GTPases and might control growth cone lamellipodia and filopodia formation in response to Rac signaling during axon pathfinding. The molecular linkage between Racs and UNC-115 in these events is unclear, and molecules that interact physically with UNC-115 remain to be identified. Furthermore, while some Rac inhibitors are known, it will

[1]*Present address:* Dana-Farber Cancer Institute, 44 Binney St., Smith 870, Boston, MA 02115.

[2]*Corresponding author:* Department of Molecular Biosciences, University of Kansas, 1200 Sunnyside Ave., 5049 Haworth Hall, Lawrence, KS 66045. E-mail: erikl@ku.edu

be important to identify all of the molecules that regulate Rac activity to precisely control distinct morphogenetic events.

To identify molecules that act with Rac and UNC-115 in axon pathfinding and cell migration, the LIM domains of UNC-115 were used as bait in a yeast two-hybrid screen of a *C. elegans* cDNA library. This screen identified a novel, conserved molecule called SWAN-1 (*s*even-*W*D-repeat protein of the *AN*11 family-1), which consists of at least seven WD repeats and a conserved C-terminal tail. In two-hybrid and pull-down assays, SWAN-1 was found to interact both with the UNC-115 LIM domains and with the Racs, suggesting that SWAN-1 is a molecular linker between UNC-115 and the Racs. An array of functional tests in *C. elegans*, mammalian fibroblasts, and yeast indicate that SWAN-1 represses Rac activity. SWAN-1 displays no similarity to other known Rac negative regulators (*e.g.*, GAPs), indicating that SWAN-1 represents a previously unidentified class of negative regulators of Rac GTPases.

MATERIALS AND METHODS

***C. elegans* culture and genetics:** *C. elegans* were cultured using standard techniques (Epstein and Shakes 1995). All experiments were performed at 20°. The *swan-1(ok267)* mutation was isolated by the *C. elegans* Gene Knockout Consortium (kindly provided by G. Molder and B. Barstead) and was outcrossed to wild type three times before phenotypic analysis. The homozygosity of *swan-1(ok267)* in all outcrosses and single and double mutants was confirmed by single-animal polymerase chain reaction (PCR) using primers that amplify a band specific to the *ok267* deletion. Germline transformation of *C. elegans* was performed by standard techniques involving injection of a DNA mixture into the syncytial germline of *C. elegans* hermaphrodites (Epstein and Shakes 1995). RNA-mediated gene knockdown (RNAi) was performed by feeding nematode strains *Escherichia coli* expressing double-stranded RNA complementary to either *swan-1* or *swan-2* (Timmons *et al.* 2001; Kamath and Ahringer 2003).

Numbers of cell corpses in the region of the pharynx at the mid-threefold stage of embryogenesis (~750 min postfertilization) were counted using differential interference contrast microscopy. Gonadal distal tip cell migration defects were scored as the percentage of gonad arms that showed defective morphology as previously described (Lundquist *et al.* 2001). In Table 1, strains harboring a full-length *swan-1::gfp* transgene were scored. As a control, nontransgene-bearing siblings from the same brood were also scored and presented in Table 1.

Significance of differences of means in Table 1 were calculated using the *t*-test, and significance of differences of proportions in Table 1 and in Figures 4, 5, 7, and 8 were calculated using both the *t*-test and Fisher's exact analysis.

Molecular biology: All fragments containing coding region that were generated by PCR were sequenced to ensure that no mutations were introduced during the procedure. The sequences of all PCR primers used in this work are available upon request.

Microscopy: See the figure legends for details about each micrograph. Unless otherwise noted, all images were captured on a Leica DMRE microscope with a 40× Planapo objective and 10× magnifier using a Hamamatsu Orca C4742-94 camera and Openlab software. Images were processed in Photoshop.

UNC-115 LIM domain two-hybrid screen: Vectors for the two-hybrid system were kindly provided by S. Elledge. The coding region for the UNC-115 LIM domains was amplified by PCR and cloned in frame to the GAL4 DNA-binding domain in the vector pAS1-CYH (the "bait" construct). The yeast strain Y190 was transformed with the bait construct by standard techniques, and autoactivation of the bait construct was tested by growth on 25 mm 3-aminotriazole (3-AT) and X-Gal, which assess expression of *HIS5* and *LacZ* reporter gene expression in Y190. The bait construct showed no autoactivation: it did not allow Y190 yeast to grow on 3-AT (no *HIS5* expression), nor did blue colonies result when transgenic yeast were grown on X-Gal (no *LacZ* expression).

Y190-bait transgenic yeast were transformed with a *C. elegans* random-primed cDNA library cloned into the pACT vector that harbors the GAL4 activation domain (the library was kindly provided by R. Barstead). Yeast were plated at high density on medium containing 25 mm 3-AT and X-Gal, and colonies that were blue (indicating *HIS5* expression and *LacZ* expression) were selected for further analysis. From an estimated 2 million cDNAs screened, 2 cDNAs representing the *swan-1* locus were recovered. These 2 cDNAs did not result in autoactivation when present in Y190 without the bait plasmid, indicating that both plasmids are needed for activation.

The coding regions of the three *C. elegans rac* genes *ced-10*, *mig-2*, and *rac-2* and the non-LIM-domain-containing portion of *unc-115* were generated by PCR and fused in frame to the GAL4 DNA-binding domain in the pAS1-CYH plasmid. None of these constructs resulted in autoactivation. These constructs were then used in direct two-hybrid tests with the pACT::SWAN-1 plasmid.

Co-immunoprecipitation experiments: HeLa cells and HEK293 cells were grown to ~80% confluency and were transfected using Fugene6 (Roche, Indianapolis). The full-length *unc-115* coding region was generated by PCR and cloned in frame to enhanced green fluorescent protein (EGFP) in the pEGFP1 vector (Clontech, Mountain View, CA). The *swan-1* coding region was cloned in frame to both the Myc epitope (MYC::SWAN-1) and the 3xFLAG epitope (FLAG::SWAN-1) in the pCMV-Myc and pCMV-3xFLAG vectors, respectively (Clontech). MYC::RAC-2 and FLAG::RAC-2 plasmids were similarly constructed. In most cases, 16 μg of plasmid were used in single transfections and 8 μg of each plasmid were used in double transfections in 75-cm^2 flasks. For RAC-2 plasmids, 8 μg were used because higher concentrations led to cell inviability. After 48 hr of growth after transfection, cells were washed with ice-cold PBS and 1 ml of ice-cold lysis buffer [150 mm NaCl/10 mm Tris (pH 7.4)/1 mm EDTA/1 mm EGTA/0.5% NP-40/0.2 mm PMSF/1% protease inhibitor cocktail; Sigma, St. Louis] was added. Cells were scraped from the bottom of the flasks, incubated for 1 hr at 4° with shaking, and centrifuged for 15 min at 16,000× *g* in a microcentrifuge at 4°. Supernatants were precleared by incubating with 80 μl of pre-equilibrated protein G Sepharose bead slurry (Amersham Pharmacia Biotech, Piscataway, NJ) for 2 hr at 4°.

An 80-μl bead slurry in 1 ml ice-cold lysis buffer was preloaded with anti-Myc monoclonal antibody (BD Biosciences, Palo Alto, CA) or anti-FLAG M2 monoclonal antibody (Sigma). After 4 hr, the beads were washed four times with lysis buffer and incubated with the precleaned lysates at 4° for 12 hr. Beads were washed in lysis buffer four times and the immune complexes were eluted from the beads by boiling in 40 μl 2× SDS loading buffer with 1 mm DTT for 5 min. The supernatants were analyzed by sodium dodecyl sulfate–polyacrylamide gel electrophoresis (SDS–PAGE) and Western blots using anti-Myc, anti-FLAG, or anti-UNC-115 antibodies (see below) and HRP-labeled secondary antibodies (Kirkegaard and Perry

Laboratories, Gaithersburg, MD) with chemiluminescent autoradiography (Pierce, Rockford, IL).

Figure 1, C and D, shows co-immunoprecipitation of UNC-115 and SWAN-1 and RAC-2 and SWAN-1. For each co-immunoprecipitation experiment, the Western blot was also probed with the antibody used for immunoprecipitation to ensure that the immunoprecipitation procedure was robust (Figure 1).

Generation of an UNC-115 antiserum: The coding region for UNC-115 residues 154–527 was inserted into the pQE9 vector (QIAGEN, Valencia, CA) in frame with the RGS-6-histidine epitope, and fusion protein was produced by bacterial expression. SDS–PAGE gel fragments containing the fusion protein were used as an antigen to immunize two rabbits (Caltag Laboratories, Healdsburg, CA). On Western blots, serum from the immunized rabbits but not preimmune serum recognized a bacterially expressed glutathione-*S*-transferase (GST) fusion with the same portion of UNC-115 (data not shown) (residues 154–527, produced by inserting the *unc-115* fragment into the pGEX4T vector; Amersham Pharmacia Biotech). UNC-115-specific antibodies were purified from the antiserum by their affinity for the GST::UNC-115 fusion protein using glutathione Sepharose beads (Amersham Pharmacia Biotech). This affinity-purified polyclonal antibody recognized a single band of ~70 kDa in Western blots of lysates of *C. elegans* (the estimated size of full-length UNC-115 polypeptide is 72 kDa) (data not shown).

***swan-1* expression analysis:** The upstream region of *swan-1* excluding the initiator ATG codon (3412–7549 relative to cosmid F53C11) was amplified, inserted into the pPD95.77 GFP expression vector (kindly provided by A. Fire), and used to drive the expression of GFP in transgenic animals. A full-length fusion of the *swan-1* coding region to *gfp* was constructed by amplifying the *swan-1* upstream region and entire coding region (3412–9941 relative to cosmid F53C11) from genomic DNA and fusing this fragment in frame to *gfp* such that the transgene was predicted to encode a full-length SWAN-1 protein with GFP at the C terminus. RNAi of *swan-1* resulted in greatly reduced GFP expression from this transgene, suggesting that the transgene encodes a SWAN-1::GFP molecule (data not shown). *swan-1* expression constructs were used at 5 ng/μl in transformation experiments.

SWAN-1 transgenic assays in *C. elegans*: For the loss-of-function *swan-1(ok267)* experiments, previously described constitutively active *rac(G12V)* transgenes were used (Struckhoff and Lundquist 2003). PDE morphological defects were scored as previously described (Struckhoff and Lundquist 2003): for each genotype, the percentages of PDE neurons exhibiting ectopic neurites and ectopic lamellipodia and filopodia were determined. After construction of each transgene in the *swan-1(ok267)* background, the transgene was crossed away from *swan-1(ok267)* and axon defects were scored again to ensure that the transgene caused defects at percentages similar to those before the experiment began. This ensured that the transgenes had not been altered during the course of the experiment and the phenotypic change was due to the presence of *swan-1(ok267)*.

For the *swan-1(+)* expression experiments, new transgenes were constructed that contained a plasmid harboring the swan-*1(+)* genomic region (bases 3412–9972 inclusive of cosmid F53C11), a *rac(G12V)* plasmid, or both. In all cases an *osm-6::gfp* plasmid was included as a neuronal marker to visualize the PDE neuron. When constructing transgenic strains, *rac(G12V)* plasmids were used at 1 ng/μl and other plasmids were used at 5 ng/μl. Multiple transgenic lines were generated for each experiment to ensure uniformity of results, and results from each line were accumulated to derive a percentage of PDE axon defects. In all *C. elegans* experiments, at least 100 animals were scored for each genotype. Significance of differences in proportions was calculated using the *t*-test and Fisher's exact analysis.

SWAN-1 transgenic assays in fibroblasts: Mammalian NIH 3T3 fibroblasts were grown and transformed as previously described (Yang and Lundquist 2005). Briefly, cells grown in six-well plates to ~50% confluency on polylysine-coated coverslips were transfected by addition of a mixture of the transgene DNA and the Fugene reagent. Cells were transfected with combinations of 1 μg each of the MYC::SWR-1 construct, a MYR::UNC-115 construct, and a CFP::RAC-1(Q61L) construct, which encodes an activated version of human Rac1 fused to cyan fluorescent protein (CFP) (kindly provided by T. Meyer). Cells were cotransfected with *egfp* to identify transfected cells, and cells transfected with *egfp* alone were used as a control. After transfection, cells were allowed to grow for 6 hr and deprived of serum (serum-containing medium was replaced by DMEM). Cells were grown for another 12 hr and fixed in 3.7% paraformaldehyde. The fixed cells were treated with 1 μg/ml of rhodamine-labeled phalloidin to visualize the actin cytoskeleton. Cells were mounted in 50% glycerin in PBS for epifluorescence microscopy. For each experiment, at least three transfections were performed and >100 cells were scored to ensure consistency of results.

SWAN-1 transgenic assays in yeast: All yeast were grown at 30°. For growth curve analysis, Y190 yeast strains harboring different plasmid constructs were grown in selective medium and diluted to ~0.1 OD_{600} units in YPD medium. Growth rates were monitored by sampling the OD_{600} culture densities each hour for 8 hr (see Figure 8). Each strain was tested at least twice, and standard deviations were indicated by error bars in Figure 8. To visualize the yeast actin cytoskeleton with rhodamine-labeled phalloidin, cells were grown in selective medium, diluted to ~0.1 OD_{600} units in YPD, and grown to midlog phase (0.3–0.7 OD_{600}) (cells harboring the CED-10 plasmid were assayed after 8 hr). Cells were fixed for 1 hr in 20% formaldehyde in 0.5 M potassium phosphate pH 6.5 and overnight in 4% formaldehyde in 100 mM potassium phosphate pH 6.5. Cells were washed in PBS and permeabilized in 0.2% Triton X-100 in PBS for 15 min, washed three times in PBS, incubated with rhodamine–phalloidin (1 μg/ml) and 4′,6-diamidino-2-phenylindole dihydrochloride (DAPI) (1 μg/ml) in PBS for 1 hr in the dark, washed three times in PBS, and mounted for fluorescence microscopy in PBS with 90% glycerol and 1 mg/ml 1,4-diazabicyclo[2.2.2]octane (DABCO) antifade reagent.

RESULTS

SWAN-1 interacts physically with the UNC-115 LIM domains and with Racs: UNC-115 is a cytoskeletal linker molecule composed of a C-terminal actin-binding villin headpiece domain (VHD) and three N-terminal LIM domains (Figure 1A) (Lundquist *et al.* 1998). To identify molecules that bind to the UNC-115 LIM domains, a yeast two-hybrid screen using the three UNC-115 LIM domains as bait was conducted (Figure 1A). From an estimated 2 million *C. elegans* cDNAs screened, two cDNAs were isolated that encode a novel protein that here is named SWAN-1. The presence of *swan-1* two-hybrid fusions with the UNC-115 LIM domain fusion specifically activated both HIS5 expression (data not shown) and *lacZ* expression (Figure 1B) in the two-hybrid system (see materials and methods). Both *swan-1* cDNAs contained the entire *swan-1* open reading

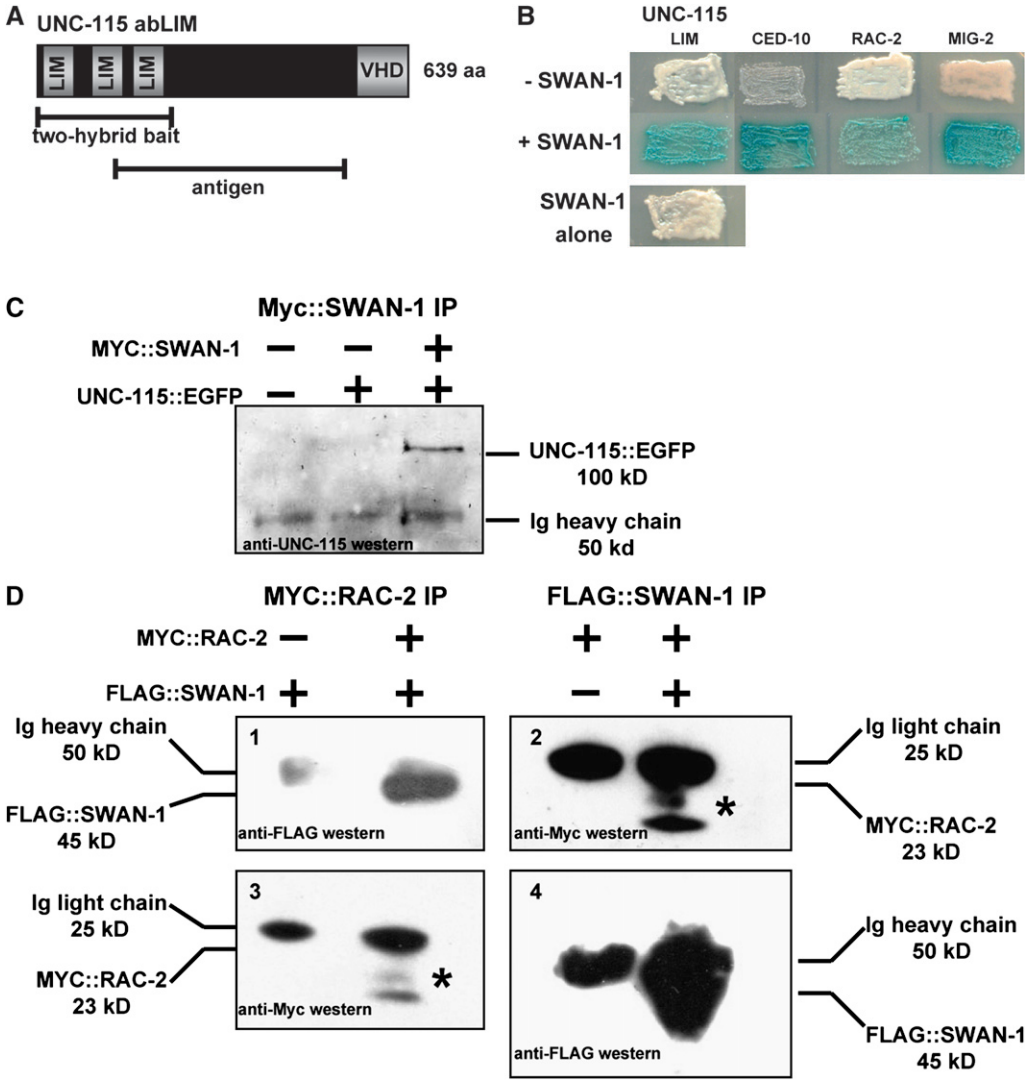

FIGURE 1.—SWAN-1 interacts with the UNC-115 LIM domains and with Rac GTPases in a two-hybrid system. (A) A diagram of the 639-residue UNC-115 polypeptide. Indicated are the regions used in the two-hybrid screen and to generate an anti-UNC-115 polyclonal antiserum. (B) Yeast harboring different bait plasmids (across the top) without and with the SWAN-1 prey plasmid (see MATERIALS AND METHODS). Yeast were grown on medium containing X-Gal to indicate *lacZ* activity and a positive interaction (blue). Yeast harboring the bait plasmids or SWAN-1 alone were overgrown to ensure absence of *lacZ* activity. Images were captured by an Epson flatbed scanner and processed in Photoshop. (C and D) SWAN-1 co-immunoprecipitated with UNC-115 and RAC-2 in HeLa cell lysates. (C) A Western blot using anti-UNC-115 antiserum. Lysates were prepared from cells expressing combinations of MYC::SWAN-1 and UNC-115::EGFP. The 100-kDa UNC-115::EGFP band is indicated, as is the Ig heavy chain of the anti-Myc antibody (50 kDa), which cross-reacts with the secondary antibody. UNC-115::EGFP was co-immunoprecipitated only when MYC::SWAN-1 was present. The successful immunoprecipitation of MYC::SWAN-1 was confirmed by Western blot with an anti-Myc antibody (data not shown). (D) MYC::RAC-2 co-immunoprecipitated with FLAG::SWAN-1. Shown are Western blots from two immunoprecipitation experiments. The blots 1 and 3 are the results of a MYC::RAC-2 immunoprecipitation, and the blots 2 and 4 are the results of a FLAG::SWAN-1 immunoprecipitation. Across the top the transgenes expressed in cells are indicated for each experiment. The top two blots (1 and 2) show that FLAG::SWAN-1 co-immunoprecipitated with MYC::RAC-2 and that MYC::RAC-2 co-immunoprecipitated with FLAG::SWAN-1, respectively. The Ig heavy chain from the anti-FLAG antibody (50 kDa), also detected by the secondary antibody, and FLAG-SWAN-1 (45 kDa) were similar in size but could be distinguished (blot 1). The Ig light chain from the anti-Myc antibody (25 kDa) and MYC::RAC-2 (20 kDa) were more difficult to resolve (blots 2 and 3). In three independent experiments, MYC::RAC-2 was evident as a thickening of the band below the Ig light chain and by the smaller bands (possible degradation products of MYC::RAC-2) below 23 kDa (asterisk). The smaller products always correlated with the presence of MYC-RAC-2. Blots 3 and 4 are the controls for immunoprecipitation [MYC::RAC-2 was immunoprecipitated with anti-Myc antibody (blot 3); and FLAG::SWAN-1 was immunoprecipitated by anti-FLAG antibody (blot 4)]. FLAG::SWAN-1 co-immunoprecipitated only in the presence of MYC::RAC-2; and MYC::RAC-2 co-immunoprecipitated only in the presence of FLAG::SWAN-1.

frame, suggesting that only the full-length SWAN-1 protein is active in the two-hybrid assay. SWAN-1 interacted specifically with the UNC-115 LIM domains, but not with the remainder of the UNC-115 molecule in the two-hybrid system (data not shown).

Because UNC-115 acts genetically downstream of Rac signaling (STRUCKHOFF and LUNDQUIST 2003), it was determined if SWAN-1 could also interact with the three *C. elegans* Rac molecules in the two-hybrid system. SWAN-1 and each of the three *C. elegans* Racs, CED-10, MIG-2, and RAC-2, interacted when directly tested in the two-hybrid system (Figure 1B). SWAN-1 interacted with both wild-type RAC-2 (Figure 1B) and constitutively active, GTPase-dead RAC-2(G12V) (data not shown).

The LIM domains of UNC-115 did not interact with any of the three Racs in the two-hybrid system, nor did any other region of UNC-115 (data not shown).

To confirm the physical interactions detected in the two-hybrid system, co-immunoprecipitation of SWAN-1 with UNC-115 and RAC-2 was assayed in lysates of HeLa cells in which tagged versions of the molecules were expressed (Figure 1, C and D). EGFP-tagged full-length UNC-115 co-immunoprecipitated with Myc-tagged SWAN-1 (Figure 1C). Experiments with MYC::RAC-2 and FLAG::SWAN-1 were consistent with co-immunoprecipitation of the molecules, although MYC::RAC-2 and FLAG::SWAN-1 bands were not completely separated from the light and heavy chains of the antibodies used for immunoprecipitation on Western blots (Figure 1D). These experiments were repeated with similar results in HeLa cells and in HEK293 cells (data not shown).

SWAN-1 is a member of a novel, conserved family of seven-WD-repeat proteins: The complete sequences of the two *swan-1* cDNAs isolated in the two-hybrid screen were determined, as were the sequences of the independently derived cDNAs yk343g2 and yk326a5 (provided by Y. Kohara) (Figure 2, A and B). The splicing pattern and coding potential for each of the four cDNAs were identical. Reverse-transcription PCR was conducted on the 5′ end of the *swan-1* transcript using a 5′ primer complementary to the *trans*-spliced leader SL1, which revealed that SL1 was spliced onto the 5′-end transcript after position 7464 relative to cosmid F53C11 (Figure 2, A and B). cDNA sequences indicated that the *swan-1* transcript was polyadenylated after position 10306 relative to cosmid F53C11 (Figure 2, A and B).

The *swan-1* cDNAs can encode a 388-residue polypeptide that is predicted to contain at least seven WD-repeat elements (Figure 3, A and B) (Neer *et al.* 1994; Smith *et al.* 1999). WD repeats are conserved structural elements that form a "β-propeller" structure, with each blade of the propeller corresponding to one WD repeat (Sondek *et al.* 1996). WD repeats have no known enzymatic activity. Rather, they are thought to form a scaffold for protein–protein interaction. Many proteins with seven WD repeats have been identified, including the β-subunit of G proteins (Smith *et al.* 1999). However, SWAN-1 is a member of a novel, conserved family of WD-repeat proteins (Figure 3C). The SWAN-1 family is ancient, as obvious SWAN-1 counterparts are found in insects, mammals, protozoa, yeast, and plants (Figure 3C). SWAN-1-family members contain at least seven regions similar to the WD repeat, with a potential eighth region near the C terminus. SWAN-1-family proteins also contain a conserved C-terminal tail that is not found in Gβ or other WD-repeat proteins (Figure 3C). Generally, the first two predicted WD repeats show more variability between species than do the others.

Two SWAN-1 family members in higher plants have known functions. AN11 from petunia is a cytoplasmic molecule involved in Myc and Myb transcription factor activation and anthocyanin pigment biosynthesis in response to light (de Vetten *et al.* 1997). In Arabidopsis, the SWAN-1-like molecule TTG1 is involved in the Myb-dependent specification of trichome cells on leaves (Walker *et al.* 1999). However, the Arabidopsis genome also encodes another SWAN-1 family member, AtAN11 (Figure 3C), which is more similar to SWAN-1 than is TTG1. The role of AtAN11 is not known, nor are the roles of SWAN-1 family members in other organisms.

The *swan-1* gene corresponds to the gene F53C11.8 in the *C. elegans* genome. Immediately downstream of the *swan-1* gene is the coding region for a gene that encodes another SWAN-1 family member here named SWAN-2 (F53C11.7 in *C. elegans* genome nomenclature) (Figure 3A). The first exon in a *swan-2* cDNA is 114 nucleotides downstream of the site of *swan-1* polyadenylation (data not shown). SWAN-2 is 45% identical at the amino acid level to SWAN-1 (Figure 3C). RNA-mediated interference (RNAi) of *swan-2* in *swan-1(ok267)* had no effect on viability, fertility, or gross morphological and behavioral phenotype. Furthermore, neither RNAi of *swan-2* nor a *swan-2* deletion allele *ok964* had an effect on activated CED-10 and RAC-2 in PDE development (data not shown).

***swan-1(ok267)* suppresses *ced-10(n1993)*:** To determine the role of SWAN-1 in *C. elegans*, a deletion allele of the gene, called *ok267*, was obtained from the *C. elegans* Gene Knockout Consortium (kindly provided by G. Molder and B. Barstead). The *swan-1* region from *ok267* mutants was amplified by PCR and sequenced to determine the breakpoints of the deletion. The 1189-bp *ok267* deletion encompassed bases 7846–9034 relative to cosmid F53C11 (Figure 2, A and B). To ensure that the wild-type *swan-1* locus had not been duplicated in the *ok267* deletion strain, PCR was performed on *swan-1(ok267)* genomic DNA using primers that were predicted to amplify a fragment in wild type but not in *swan-1(ok267)* (one primer was complementary to a region removed by *ok267*). These primers amplified a fragment from wild type but not from *swan-1(ok267)* (data not shown).

The *ok267* deletion removed the coding region for 223-amino-acid residues of the 388-residue SWAN-1 polypeptide, including all of WD repeats two to six and part of seven (Figure 3, A and B). *swan-1(ok267)* animals were viable and fertile and displayed no apparent phenotype, including gross morphological or behavioral defects. RNAi directed against *swan-1* had no detectable phenotype. Furthermore, no *swan-1* transcript was detected by RT–PCR in *swan-1(ok267)* mutants (data not shown).

Because SWAN-1 interacted physically with UNC-115 and the Racs, double mutants of *swan-1(ok267)* were built with the *rac* pathway mutants *ced-10* (Lundquist *et al.* 2001), *mig-2(mu28)* (Zipkin *et al.* 1997), *unc-73* (Steven *et al.* 1998), and *unc-115* (Lundquist *et al.* 1998). *swan-1(ok267)* suppressed cell corpse phagocytosis and gonadal distal tip cell migrations of *ced-10(n1993)*

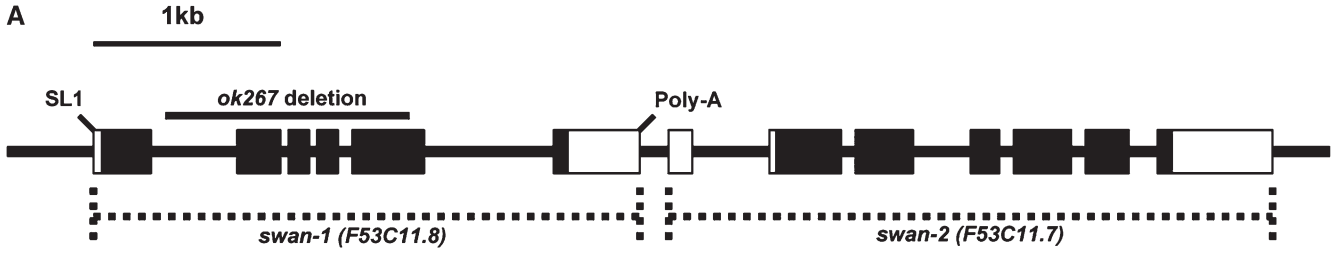

B

```
AAACTTGTGAACCCTTATCACCTGCAATGGCTACCAATGGTCACGCAGTG          aaacgaatgctgaaagagaactttcaaaagttgacactaacgattacaaa
AACGGAGAAGCTCATGTTATGCAACAAGTCGCACAACAACCAGCTCCACC          aaaaaaacatttacacgcagttatttgaatttaattataaaaatctcatt
AGGACCATTAGCTCCGCAAGGGATCGGAAGACAGAACGAAATTGTGATCG          cattcattgaacattttacctgaaaattgaataaaaaggtaaaaaaggtg
GAGGACGTGATCGACGTTGTGAGATCTATAAATTCACGTCTGATCAACAG  200     Cgtccctttttgttaatttttgcatcaaattttcttatatttcttagaa  2000
TTGTATGCATCGGCATGGAGCAACAAAAATGATATCAAATTTCGACTTGC          ttttacataatttctacaatgtcactagtgggactcagaggtgcagtct
TGTGGGAACAGTATCCGACGTGTCCGTTAACCCATGTGCCGCAAACAAGg          taaaaattgcaagtaatgagccactttgaaaactggaatatttgagatct
tgagtttttgaaaaatttgaaaacgtgtgagtggtaatgttggccatagt          gagagtttaaaaactgtttttcgaagcggattgtttttattctaccatgt
Caataaggtcccatttactgaaatacccacaaaaaacgcaattctaaaaaa  400     Ttacattacatttgctgaaacagttaacaattacatccaagttttttctt  2200
cgggtttttgcaaattctaatctactgtttaagttgtctacaaaataaga          ctatgccgaacttagcttggctccgttttcggggtgaatttttttccacc
actgcaagattaaacagcgatcgttcttatttttgagttgagttatattt          tgcttttccggaatcataaacatcgaagtttcatactacgttcagctgtt
ttgagtcgagttttactatagttcaaagacacaatttagaaaaactggaa          gcacgtagtttcttagaaaacataaactatgaattgtcacctaaattttg
Atcggaacaaatcgaaattgaactgttcaggttttaaacataatttttgt  600     ttggagatttccagtttcaaaactttcattactatacaatttccagGTCA  2400
ctttccttttgcggtatttcagtatgtatattaaaacatttcgaatattt          ATCAAATTCATTGGGGTCCTGTACACAGTAACTGGATTGCAATTTGCTTC
tgaattgaaaaccctatagactgtactccaatgtaaaagttaaaaaaaaa          AACAAAACTCTTGAGATTCTTCGAGTTTGAGCAGAGGATGTGCGTTCTGT
aaaaacgaaatttatatgtattttgaaacataacagttccaattaaaacg          TTGAGAACTAACAAAAATTTCTCACATTTCTCAATTAACGTTATTTTCCA
ttttcagGTATCAATTGTACAACTAAAAGACGAAACTGGCGAGCTTGTCG  800     TTTCCTGTTATGTTTTTATGTTTTTAAATTATAATTTTTTGTCAATTGCT  2600
AGACGGCGAGCTTTCCAATGGAGTTCCCAGCCAATGCAGTCGGTTTTATT          CTGATTTCAAGTCACTTTCTCCGCCTTTGTTGTGAACAACTTATTTGAAT
CCGGATCCAGACAACGTTTACCCTGATCTCATTGCCACAACATCAGATTG          TAATTCCAAAGCATCAGTATGATGATTCACGATCTCTTTCAAACCTCAAT
CCTTCGCCTCTGGCGAGTAGTTGATGGAAAAGTTCATCCAGACGCAGTTA          TTTCTCACGCCAACACACAATTGTTTTATCCACCCGAAAATTATTGTTTT
TGATCAATAATACTgtacgttaaacctgtaaatttttagtgttcaatgga  1000    ATATCCTATTTTTTTCCATTTTCCATTGTGATAAGGTTACAGGAAACCCG  2800
attttcagAACTCACAATATGGATCAGCTTTGACAAGTTTCGACTGGAAC          AAAATTTTTTAAGGTGGTTTCAAAAAAAATTTCAGAAATTGT          2842
GAGCTGGAGCCGAGGTATATTGGAGTTTCCAGTGTAGATACGACTTGCAC
AATTTATGATGTTGAGgtgagttataattttgataagatttagtgaaatg
tttacaaatattcagGTTGGTTGCGCAATTGGGCAGACCAAGCCGACAGC  1200
TCCATTCACACTCAAAACACAACTGATTGCTCATGACAAGCCTGTTCACG
ATATCGAATTTGCTAAAATCAATGGCGGTCGTGATCATTTTGCAACTGTT
Ggtgagtcttgtctagctagtatttgcatcttttataaacattacgagt
ttccagGAGCTGACGGAAGTGCCCGAATGTTTGATCTTCGACATTTAAAC  1400
CACTCGACAATTGTCTATGAAGATCCAAACAAGGAGAAGCTTCAAAGACT
GTCATGGAACAAACAAGAACCTTATTTCATGGCTTTATTTGCCGAGAACA
GTCAAGAAGTTCAAATTCTTGACATTCGTATGCCATGCAACATTCTCTGT
CGACTCCGTAATCACACTGGACCAGTGAACGGAATTGCATGGGCCCCACA  1600
CAGTCCACATCACATTTGTACTGCTGGAGACGATTCACAAGCTCTGATTT
GGGATCTGCAGCAGGTTCCAAGACCCGTTGATGATCCGATTCTGGCTTAT
TCGGCTGGTGGAGAGgtgagcatttgaatttgaacttaaaatcttatccg
atcaagatcaaaaagtagtgagattaaaaaatatatatacctgaaaatta  1800
```

FIGURE 2.—The *swan-1* locus. (A) A depiction of the *swan-1* and *swan-2* loci (5′ is to the left). Boxes represent exons; solid boxes represent coding regions. SL1 indicates where the *trans*-spliced leader sequence SL1 is attached to the 5′ end of the *swan-1* cDNA; and the site of a poly(A) tail on the *swan-1* cDNA is shown. The extent of the *swan-1(ok267)* deletion is indicated. (B) The *swan-1* coding region. Uppercase letters represent exons present in three independent cDNAs that were sequenced, and bold letters represent the open reading frame. Lower case indicates intron sequences inferred from the sequence for the F53C11.8 region on WormBase. Underlined sequences represent the extent of the *ok267* deletion. Base 1 of the sequence is where an SL1 trans-spliced leader sequence is present in a cDNA generate by 5′ RACE. The two arrows represent the start points of two independent cDNAs isolated in the yeast two-hybrid screen. The sequences of these two cDNAs as well as those of two other independently-derived cDNAs yk326a5 and yk343g2 (kindly provided by Y. Kohara) were determined and were identical throughout the open reading frames of the cDNAs. The end of the sequence is where a poly(A) tail is present in yk1174f05 (data from WormBase).

and enhanced axon defects caused by activated Rac molecules (see below). No effects were observed in *swan-1(ok267)* double mutants with *unc-73* or *unc-115* (data not shown).

ced-10 Rac mutations cause defects in phagocytosis of cells undergoing programmed cell death (REDDIEN and HORVITZ 2000) and defects in the migration of the gonadal distal tip cells (LUNDQUIST *et al.* 2001), resulting in malformed gonads. *swan-1(ok267)* significantly suppressed the cell corpse engulfment defects and the gonadal distal tip cell (DTC) migration defects of *ced-10(n1993)* mutants (Table 1). *ced-10(n1993)* mutants alone displayed 14.9 ± 3.8 persistent cell corpses in the pharyngeal region of late threefold-stage embryos, compared to 9.6 ± 4.2 in *swan-1(ok267); ced-10(n1993)* double mutants ($P < 0.001$). Furthermore, 24% of *ced-10(n1993)* mutants displayed misshapen gonads due to DTC migration errors, whereas *swan-1(ok267);*

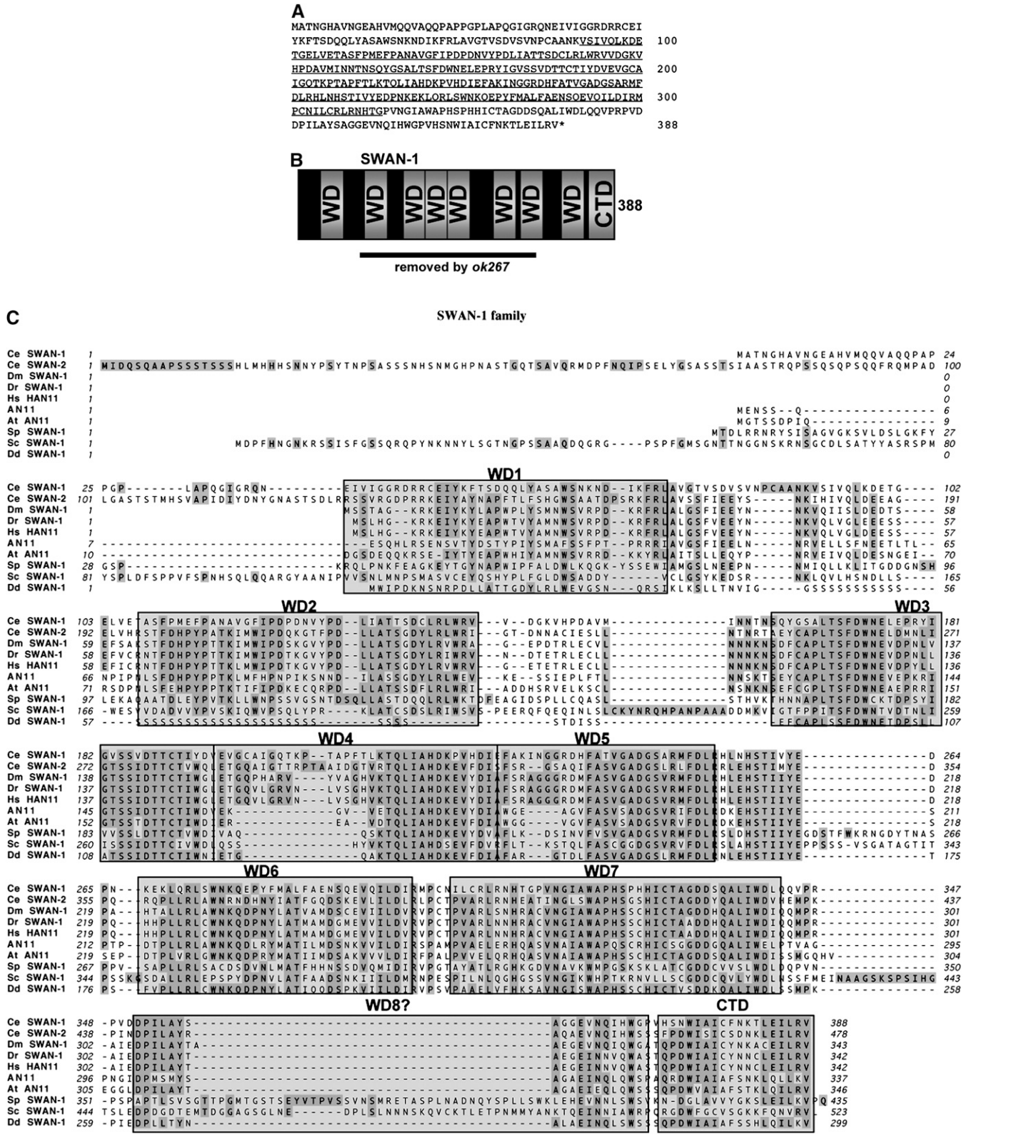

FIGURE 3.—The SWAN-1 polypeptide. (A) The amino acid sequence of the 388-residue SWAN-1 polypeptide. Residues whose coding region was removed by the *ok267* deletion are underlined. (B) Schematic of the SWAN-1 polypeptide. Regions with similarity to the WD repeat domain are indicated, as is the C-terminal conserved domain (CTD) unique to SWAN-1-family polypeptides. The region of the molecule whose coding region was removed by *ok267* is indicated. (C) The SWAN-1 family is conserved in animals, plants, fungi, and protozoa. Predicted amino acid sequences were aligned by ClustalW: Ce, *C. elegans* SWAN-1 (GenBank accession no. NP_506418) and SWAN-2 (NP_506417); Dm, *Drosophila melanogaster* (NP_608461); Dr, *Danio rerio* (zebrafish)

(*continued*)

TABLE 1

swan-1* loss of function suppresses *ced-10(n1993)* but not *mig-2(mu28)

Genotype	No. of persistent cell corpses/embryo[a]	% distal tip cell migration defects[b]
+	0.05 ± 0.3	0
	$n = 50$	$n > 200$
swan-1(ok267)	0.1 ± 0.3	3 ± 1
	$n = 56$	$n = 132$
ced-10(n1993)	14.9 ± 3.8[c]	24 ± 4[d]
	$n = 97$	$n = 120$
ced-10(n1993); swan-1(ok267)	9.6 ± 4.2[c]	7 ± 2[d]
	$n = 89$	$n = 113$
ced-10(n1993); swan-1(ok267); Ex[swan-1(+)][e]	15.6 ± 3.4[f]	29 ± 3[g]
	$n = 119$	$n = 191$
ced-10(n1993); swan-1(ok267) (non-transgene-bearing sibs)[e]	11.7 ± 3.6[f]	12 ± 2[g]
	$n = 115$	$n = 174$
mig-2(mu28)	NA	16 ± 3
		$n = 145$
mig-2(mu28); swan-1(ok267)	NA	17 ± 4
		$n = 101$

[a] Persistent corpses in the region of the pharynx were scored in threefold larvae prior to hatching (~750 min postfertilization) (± standard deviation).

[b] In young adult hermaphrodites, distal tip cell migration was scored as defective if the gonad arm failed to execute its complete migration or if the gonad arm was misguided (± standard error of the proportion).

[c] Distributions are significantly different (*t*-test, $P < 0.001$).

[d] Proportions are significantly different (*t*-test and Fisher's exact analysis, $P < 0.001$).

[e] *Ex[swan-1(+)]* is a transgenic array harboring wild-type *swan-1*. Non-transgene-bearing sibs are the siblings of transgenic animals from the same brood that did not inherit the transgene.

[f] Distributions are significantly different (*t*-test, $P < 0.001$).

[g] Proportions are significantly different (*t*-test and Fisher's exact analysis, $P < 0.001$).

ced-10(n1993) double mutants displayed 7% ($P < 0.001$). *swan-1(ok267)* alone had little effect on cell corpse engulfment or DTC migration on its own (Table 1). *ced-10(n1993)* is a hypomorphic allele that retains some *ced-10* activity (Reddien and Horvitz 2000; Shakir *et al.* 2006). That *swan-1(ok267)* suppressed the defects caused by *ced-10(n1993)* suggests that the normal role of SWAN-1 might be to repress CED-10 Rac activity [*i.e.*, in the absence of SWAN-1, the remaining activity of *ced-10(n1993)* is increased]. While *swan-1* slightly suppressed the hypomorphic *ced-10(n1993)* allele, it did not suppress the maternal-effect lethality or gonad defects of the *ced-10(n3417)* null allele nor did it suppress the lethality or axon pathfinding defects associated with the *ced-10(n1993); mig-2(mu28)* double mutant (data not shown).

To confirm that the suppression of *ced-10(n1993)* was due to the *swan-1(ok267)* deletion, a full-length *swan-1::gfp* transgene (predicted to encode a full-length SWAN-1::GFP fusion protein; see materials and methods) was analyzed for its ability to rescue suppression by *swan-1(ok267)*. The *swan-1::gfp* transgene rescued the effects of *swan-1(ok267)* suppression in *ced-10(n1993); swan-1(ok267)* mutants (Table 1): transgene-bearing *ced-10; swan-1* animals displayed 15.6 ± 3.4 persistent cell corpses and siblings that did not inherit the transgene displayed 11.7 ± 3.6 persistent cell corpses ($P < 0.001$). Furthermore, suppression of DTC migration defects was rescued (29% *vs.* 12%, respectively; $P < 0.001$) (Table 1).

Mutations in the *mig-2 Rac* gene also cause DTC migration defects (Lundquist *et al.* 2001). *swan-1(ok267)* did not suppress the DTC migration defects of *mig-2(mu28)* (Table 1). As opposed to *ced-10(n1993)*, which retains some CED-10 function, *mig-2(mu28)* is a null allele that likely causes complete loss of *mig-2* function. This might explain why *swan-1(ok267)* did not suppress *mig-2(mu28)*. Indeed, evidence is presented below that SWAN-1 can regulate MIG-2.

***swan-1(ok267)* enhances constitutively active Rac in neurons:** To further test the idea that SWAN-1 is a negative Rac regulator, the effect of *swan-1* loss of function

(NP_956363); Hs, *Homo sapiens* (AAH01264); AN11 from *Petunia x hybrida* (AAC18914); At, *Arabidopsis thaliana* (NP_172751); Sp, *Schizosaccharomyces pombe* (CAA21079); Sc, *Saccharomyces cerevisiae* (NP_015077); Dd, *Dictyostelium discoideum* (protozoan slime mold) (XP_643620). Residues identical in a majority of the molecules are highlighted in dark shading. Regions similar to the WD repeat (WD1–8) and the conserved C-terminal domain (CTD) are boxed in light shading. Members from the yeast *S. cerevisiae* and *S. pombe* include additional amino acid residues, not found in other members, between WD5 and WD6, between WD7 and WD8, and in WD8. The SWAN-1-like molecule from the protozoan *D. discoideum* contains a run of 38 consecutive serines in the region that corresponds to WD2.

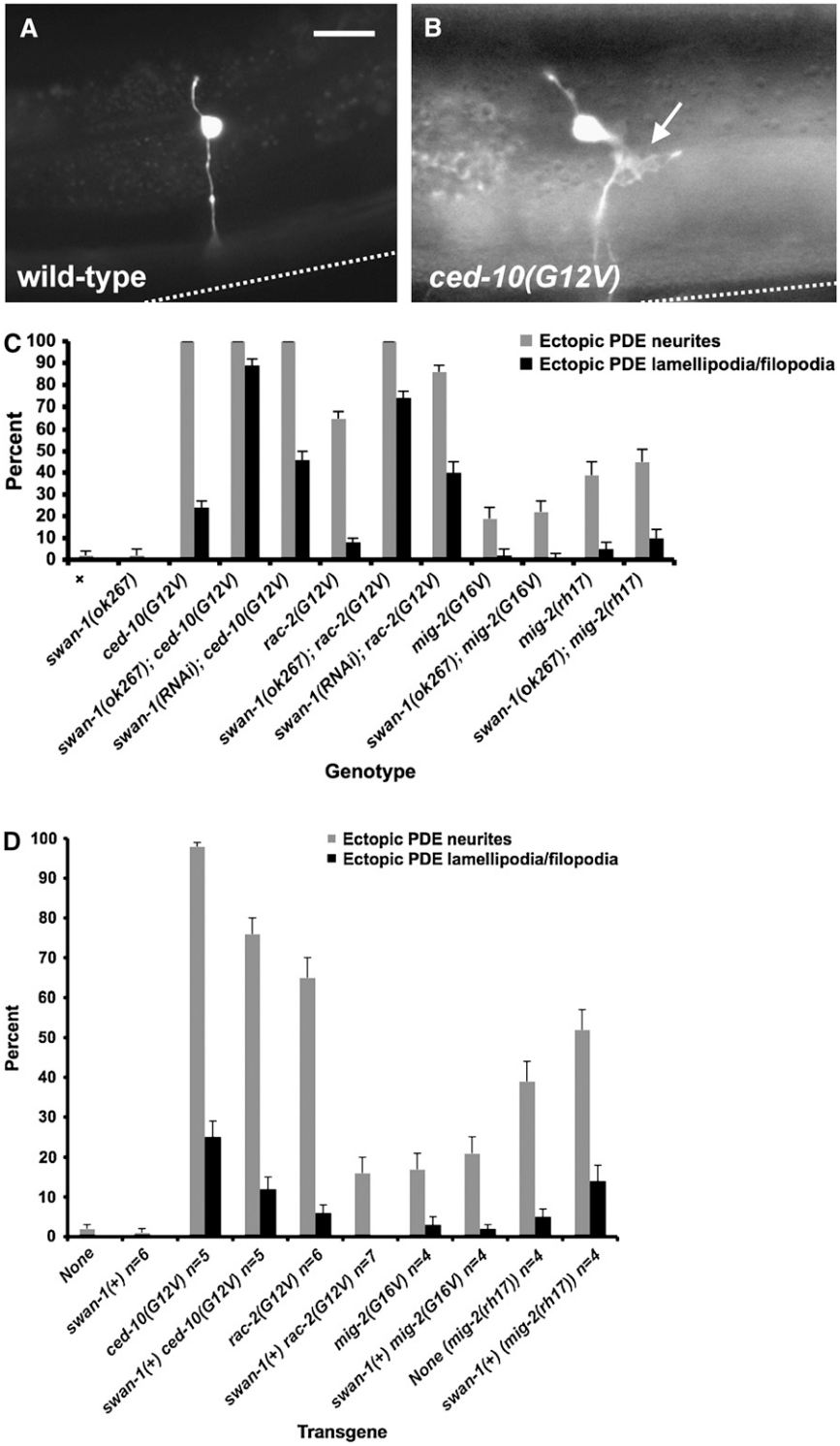

FIGURE 4.—SWAN-1 negatively modulates activated Rac. (A and B) Fluorescence micrographs of the PDE neurons of young adult animals with *gfp* expression driven by the *osm-6* promoter in the PDE neuron. Anterior is left and dorsal is up; bar in A, 5 μm. (A) Wild-type PDE morphology. A ciliated dendrite extends dorsally, and a single unbranched axon extends ventrally to the ventral nerve cord (out of focus; dashed line). (B) A PDE neuron with CED-10(G12V) expression. The neuron displayed ectopic protrusive structures that resemble lamellipodia and filopodia. Ectopic axons and axon branches were also observed (data not shown). (C) Loss-of-function *swan-1(ok267)* enhances the effects of activated CED-10(G12V) and RAC-2(G12V) transgenes. Genotypes analyzed define the *x*-axis, and the percentages of PDE neurons displaying ectopic lamellipodia/filopodia and ectopic neurites define the *y*-axis. Error bars represent the standard error of the proportion. (D) Transgenic expression of wild-type *swan-1* suppresses transgenic CED-10(G12V) and RAC-2(G12V). The *x*-axis is compositions of transgenes analyzed. Transgenes included activated *rac(G12V)* constructs with and without wild-type *swan-1* DNA (see MATERIALS AND METHODS). Multiple transgenic lines (*n*) were analyzed for each combination. The *y*-axis and error bars are as described in C. As determined by a *t*-test and by Fisher's exact analysis, the effects of *swan-1(ok267)*, *swan-1(RNAi)*, and *swan-1(+)* expression on CED-10(G12V) and RAC-2(G12V) were significant ($P < 0.001$).

on Rac activity in development of the PDE neurons was studied. The PDEs are a pair of ciliated sensory neurons that reside in the posterior-lateral region of *C. elegans* in the postdeirid ganglion (WHITE *et al.* 1986; SHAKIR *et al.* 2006). A single ciliated dendrite extends dorsally from the cell body, and a single axon extends ventrally to the ventral nerve cord, where it branches and runs anteriorly and posteriorly (Figure 4A).

Previous studies indicated that constitutively active Rac molecules, produced by the canonical glycine 12 to valine (G12V) mutation, induce ectopic neurite formation and ectopic lamellipodia and filopodia formation in the PDE neuron *in vivo* (Figure 4B) (STRUCKHOFF and LUNDQUIST 2003). *swan-1(ok267)* enhanced the effects of transgenic *ced-10(G12V)* and *rac-2(G12V)* (Figure 4C). For example, *rac-2(G12V)* caused 65% ectopic

axon formation and 8% ectopic lamellipod and filopod formation, whereas *swan-1(ok267); rac-2(G12V)* animals displayed 100 and 74% of the respective defects. While all effects of *swan-1(ok267)* and *swan-1(RNAi)* on CED-10(G12V) and RAC-2(G12V) were significant ($P < 0.001$), the effects of *swan-1* on *rac-2(G12V)* were more pronounced than those on *ced-10(G12V)*. In addition to increasing the penetrance of *rac-2(G12V)* and *ced-10(G12V)* defects, *swan-1(ok267)* also increased the severity of defects. For example, *ced-10(G12V)* PDEs generally displayed one to two ectopic axons, whereas *swan-1(ok267)l ced-10(G12V)* PDEs often displayed three or more ectopic axons. Occasionally, so many ectopic axons were present that it became impossible to distinguish which axon was the normal PDE axon. RNAi of *swan-1* gave similar but weaker results (Figure 4C), indicating that the effects were due to disruption of *swan-1* function. These results demonstrate that *swan-1(ok267)* enhances the effects of *ced-10(G12V)* and *rac-2(G12V)*.

The *mig-2(rh17)* mutant harbors an activating G16 mutation (Zipkin *et al.* 1997). Neither *mig-2(rh17)* nor the effects of transgenic expression of MIG-2(G16V) were significantly affected by *swan-1(ok267)* (Figure 4C).

SWAN-1(+) transgenic expression represses constitutively active Rac: If SWAN-1 is a negative Rac regulator, overactivity of wild-type SWAN-1 might repress Rac activity. Transgenic expression of wild-type *swan-1* suppressed the effects of *ced-10(G12V)* and *rac-2(G12V)* (Figure 4D; see materials and methods). For example, *rac-2(G12V)* trangenes averaged 65% ectopic PDE axons and 6% ectopic lamellipodia and filopodia, whereas *rac-2(G12V)* transgenes that also contained wild-type *swan-1* DNA averaged 16 and 0% defects, respectively. While all effects of SWAN-1(+) expression on CED-10(G12V) and RAC-2(G12V) were significant ($P < 0.001$), suppression of *ced-10(G12V)* was weaker than that of *rac-2(G12V)*. *swan-1* coexpression had no detectable effect on *mig-2(G16V)* (Figure 4D).

***swan-1(ok267)* enhances the neuronal effects of dominant *Rac* alleles:** In contrast to *ced-10(n1993)* and *mig-2(mu28)*, the mutations *ced-10(n3246)*, *ced-10(n1993lq20)*, *mig-2(rh17)*, and *mig-2(lq13)* all cause axon defects on their own, indicating that they are not simple loss-of-function mutations (Shakir *et al.* 2006). *mig-2(rh17)* affects the glycine 17 residue of the MIG-2 protein (Zipkin *et al.* 1997) and is likely to result in constitutively active, GTPase-dead MIG-2 [the equivalent mutation was included in the *mig-2(G16V)* transgenes]. It is unknown whether *ced-10(n3246)*, *ced-10(n1993lq20)*, or *mig-2(lq13)* are activating or dominant-negative mutations.

swan-1(ok267) enhanced the axon defects caused by each of these dominant *Rac* alleles. *ced-10(n3246)*, *ced-10(n1993lq20)*, *mig-2(rh17)*, and *mig-2(lq13)* caused a variable PDE axon pathfinding phenotype that was categorized as mild (the axon reaches the ventral nerve cord near the normal position but is misguided) or severe (the axon fails to reach the ventral nerve cord near the normal position) (Figure 5, A and B). The percentages of combined mild and severe axon defects of *swan-1(ok267)* double mutants with *ced-10(n3246)*, *mig-2(lq13)*, and *mig-2(rh17)* were increased, and the severity of all four increased ($P < 0.001$; Figure 5C). For example, *ced-10(n3246)* alone showed 8% axon defects, most of which were of the mild class, and *swan-1(ok267); ced-10(n3246)* showed 18% defects with 8% of the severe class.

***swan-1* is expressed in many cell types including neurons:** To further understand the role of *swan-1* in *Rac* signaling, the temporal and spatial pattern of *swan-1* expression during development was analyzed. Two *swan-1* expression transgenes were constructed: a transcriptional reporter consisting of the *swan-1* promoter driving green fluorescent protein (*gfp*) expression and a translation reporter of the full-length *swan-1* region fused in frame to *gfp* such that a full-length SWAN-1 molecule fused to GFP at the C terminus is produced (SWAN-1::GFP) (see materials and methods). Full-length *swan-1::gfp* expression was first detected at ~100 min postfertilization when embryonic transcription begins. Expression was observed in most cells (Figure 6, A–C), including neuroblasts and neurons, and persisted throughout development into adulthood. The only cells that did not show *swan-1::gfp* expression were the intestinal cells and their precursors (Figure 6, A–C). SWAN-1::GFP accumulated predominantly in the cytoplasm of all cell types analyzed. The transcriptional reporter transgene displayed a temporal and spatial expression pattern identical to that of the full-length fusion transgene (data not shown).

SWAN-1 represses human Rac1 in 3T3 fibroblasts: The above data indicate that SWAN-1 represses Rac activity in *C. elegans* neuronal morphogenesis. CED-10 Rac and RAC-2 Rac are very similar to human Rac1 (83% identical at the amino acid level) (Lundquist *et al.* 2001). Expression of constitutively active Rac1 (the glutamine to leucine mutation at position 61, Q61L) in serum-starved 3T3 fibroblasts led to lamellipodial membrane protrusions along cell edges (Figure 7A). We found that 62% of 3T3 cells expressing Rac1(Q61L) exhibited lamellipodial plasma membrane extensions (Figure 7, A and B) not seen in *egfp* control-transfected cells. Expression of myc-tagged SWAN-1 alone had little effect on cell morphology (Figure 7B). Fewer cells transfected with both Rac1(Q61L) and SWAN-1 displayed lamellipodial structures (26% compared to 62% for Rac1 alone; $P < 0.001$) (Figure 7B), suggesting a partial suppression of Rac1(Q61L) activity by SWAN-1.

SWAN-1 might directly repress Rac activity. Alternatively, SWAN-1 might inhibit downstream Rac effectors, such as UNC-115. In *C. elegans* neurons, no repression of activated UNC-115 by SWAN-1 was detected (data not shown). As previously reported, addition of an N-terminal myristoylation sequence (Myr) from human

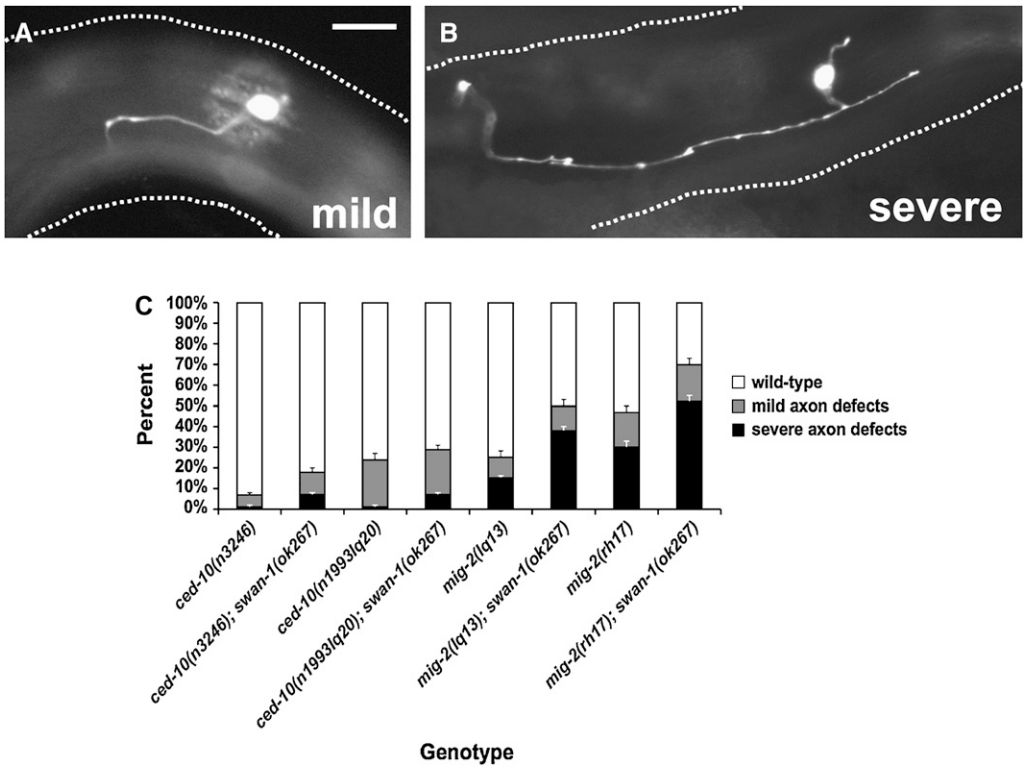

FIGURE 5.—*swan-1(ok267)* enhances dominant *ced-10* and *mig-2* alleles. (A and B) Fluorescence micrographs of *osm-6::gfp* expression in PDE neurons from *ced-10(n3246); swan-1(ok267)* animals. Anterior is left and dorsal is up; bar in A, 5 μm. Dashed lines indicate the dorsal and ventral limits of the body of the animal. (A) A mild PDE axon pathfinding defect, where the axon is misguided but reaches the ventral nerve cord (out of focus; dashed line) in the vicinity of the cell body. (B) A severe PDE axon pathfinding defect, where the axon fails to reach the ventral nerve cord. (C) Genotypes analyzed define the *x*-axis, and the *y*-axis represents the percentage of PDE neurons in each genotype displaying wild-type morphology (open bars), mild axon pathfinding defects (shaded bars), and severe axon pathfinding defects (solid bars). Open error bars represent the standard error of the proportion of severe axon defects, and solid error bars represent standard error of the proportion of combined mild and severe defects. Differences in the severe category between the activated *rac* mutation alone and the double with *swan-1(ok267)* were significant ($P < 0.001$; *t*-test and Fisher's exact analysis).

c-Src targeted UNC-115 to the plasma membrane and caused overactivation of UNC-115, resulting in ectopic lamellipodia and filopodia formation in serum-starved fibroblasts (Figure 7C). In 24% of MYR::UNC-115-expressing cells, lamellipodial and filopodial membrane protrusions were observed (Figure 7, C and D). Cotransfection of SWAN-1 with MYR::UNC-115 resulted in 15% of cells exhibiting protrusive morphology, a difference that was not statistically significant ($P = 0.1076$). While these data indicate that SWAN-1 might slightly repress UNC-115, the effect is not as pronounced as the effect of SWAN-1 on Rac1.

SWAN-1 represses Rac activity in yeast: In the course of the directed two-hybrid experiments using SWAN-1 and the Racs, it was noted that yeast transformed with CED-10 and MIG-2 (but not RAC-2) were slow-growing and formed small and irregular-shaped colonies. The doubling times of strains harboring CED-10 and MIG-2 grown in liquid culture were increased compared to that of the parent strain Y190 (Figure 8A). CED-10 cells had a doubling time of >10 hr and MIG-2 cells had a doubling time of ~6 hr, compared to ~2.5 hr for Y190. Doubling time compared to that of Y190 was not significantly affected by RAC-2 or SWAN-1 expression (data not

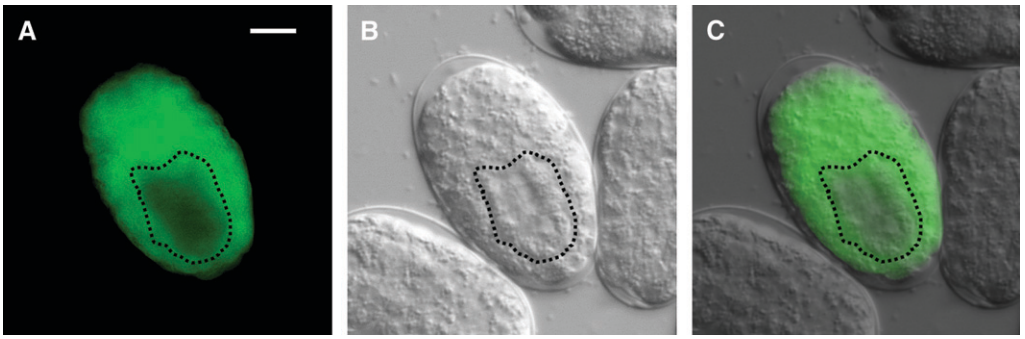

FIGURE 6.—*swan-1::gfp* is expressed in all cells except the intestine. Micrographs of an embryo, ~270 min after fertilization, harboring the full-length *swan-1::gfp* fusion transgene are shown (see MATERIALS AND METHODS). An HCX Planapo 63× objective (1.3 numerical aperture) and a 10× magnifier were used. The dashed line surrounds the intestinal precursor cells. Bar in A, 10 μm. (A) A fluorescence micrograph; (B) a differential interference contrast micrograph; (C) a merged image.

shown). When cell morphology was analyzed, fewer of the CED-10 and MIG-2 cells were in the process of budding during the log phase of growth compared to the parent Y190 strain (Figure 8B). For example, 85% of Y190 cells were in the process of budding whereas 29% of CED-10 and 45% of MIG-2 cells were budding.

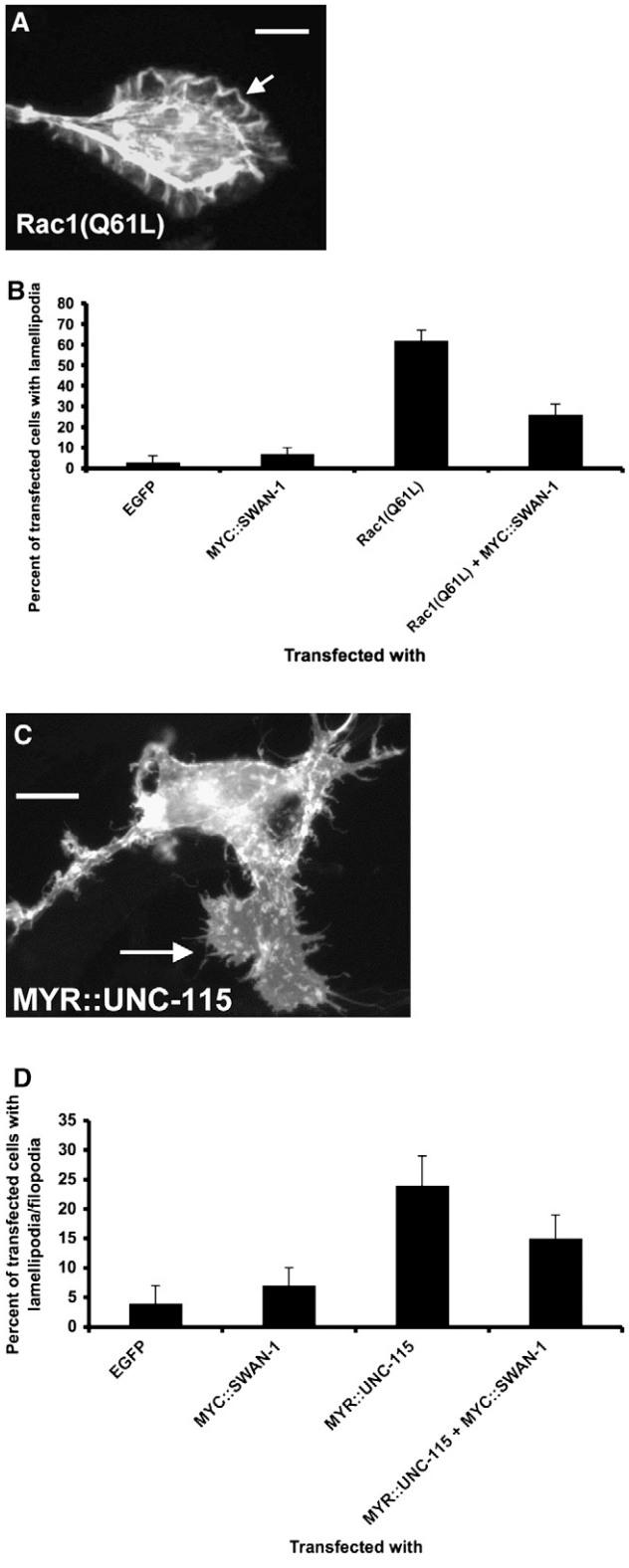

SWAN-1 and RAC-2 expression had little effect on percentage of cells undergoing budding (Figure 8B).

CED-10- and MIG-2-expressing cells displayed abnormal morphology, including greatly increased cell size and irregular cell shape (18/21 of CED-10-expressing cells and 24/30 MIG-2-expressing cells). Phalloidin staining revealed that the actin cytoskeleton was disorganized in these cells. In normal budding cells, the actin cytoskeleton is dramatically polarized; the newly forming bud displays actin patches on the cell surface as a result of endocytosis involved in bud growth; and long actin filaments extend from the mother cell to the bud (Adams and Pringle 1984). The actin cytoskeleton of the host strain Y190 displayed this morphology characteristic of asymmetric growth and budding (Figure 8C). In CED-10 and MIG-2 cells undergoing budding, actin patches were often observed both in the bud and in the mother cell (Figure 8, D and E), indicating that cell polarity and asymmetric growth had been disrupted. Furthermore, the long actin filaments were often missing (Figure 8, D and E). When the long filaments were present, they were often disorganized with respect to the bud–mother cell axis (Figure 8D). In the large, irregular, nonbudding cells, actin patches were observed uniformly on the cell surface (Figure 8G), indicating that these cells were undergoing nonpolarized growth without budding. While most RAC-2-expressing cells had normal morphology, some with abnormal polarized growth and actin cytoskeleton disorganization were observed at a low frequency (Figure 8F), which apparently did not significantly interfere with the growth dynamics of RAC-2-expressing yeast. SWAN-1-expressing cells showed no apparent morphology and cytoskeletal defects (data not shown).

The observed defects in budding, polarized growth, and actin disorganization mirrored those seen in selected mutants of the six yeast Rho GTPases (Rho1–5p

Figure 7.—SWAN-1 inhibits human Rac1 activity in cultured cells. (A) A serum-starved NIH 3T3 fibroblast transfected with activated human Rac1(Q61L), fixed and stained with rhodamine–phalloidin to visualize the actin cytoskeleton. The arrow indicates a lamellipodial ruffle surrounding the cell. (B) The combinations of transgenes used to transfect serum-starved fibroblasts define the *x*-axis. EGFP was included in each mix. Rac1 harbored the Q61L mutation, and SWAN-1 was tagged with the Myc epitope. The percentage of transfected cells (as judged by the EGFP expression) displaying lamellipodia define the *y*-axis. Error bars represent standard error of the proportion. The effects of SWAN-1 expression on Rac1(G12V) activity were significant ($P < 0.01$) as judged by a *t*-test and Fisher's exact analysis. (C) A fluorescence micrograph of a serum-starved fibroblast harboring a MYR::UNC-115::EGFP transgene. Fluorescence is from MYR::UNC-115::EGFP. The arrow indicates a large lamellipodial protrusion with multiple filopodia. D is as described in B. The effects of SWAN-1 expression on MYR::UNC-115 activity were not significant as judged by a *t*-test ($P = 0.1076$) and Fisher's exact analysis. Bar in A, 5 μm.

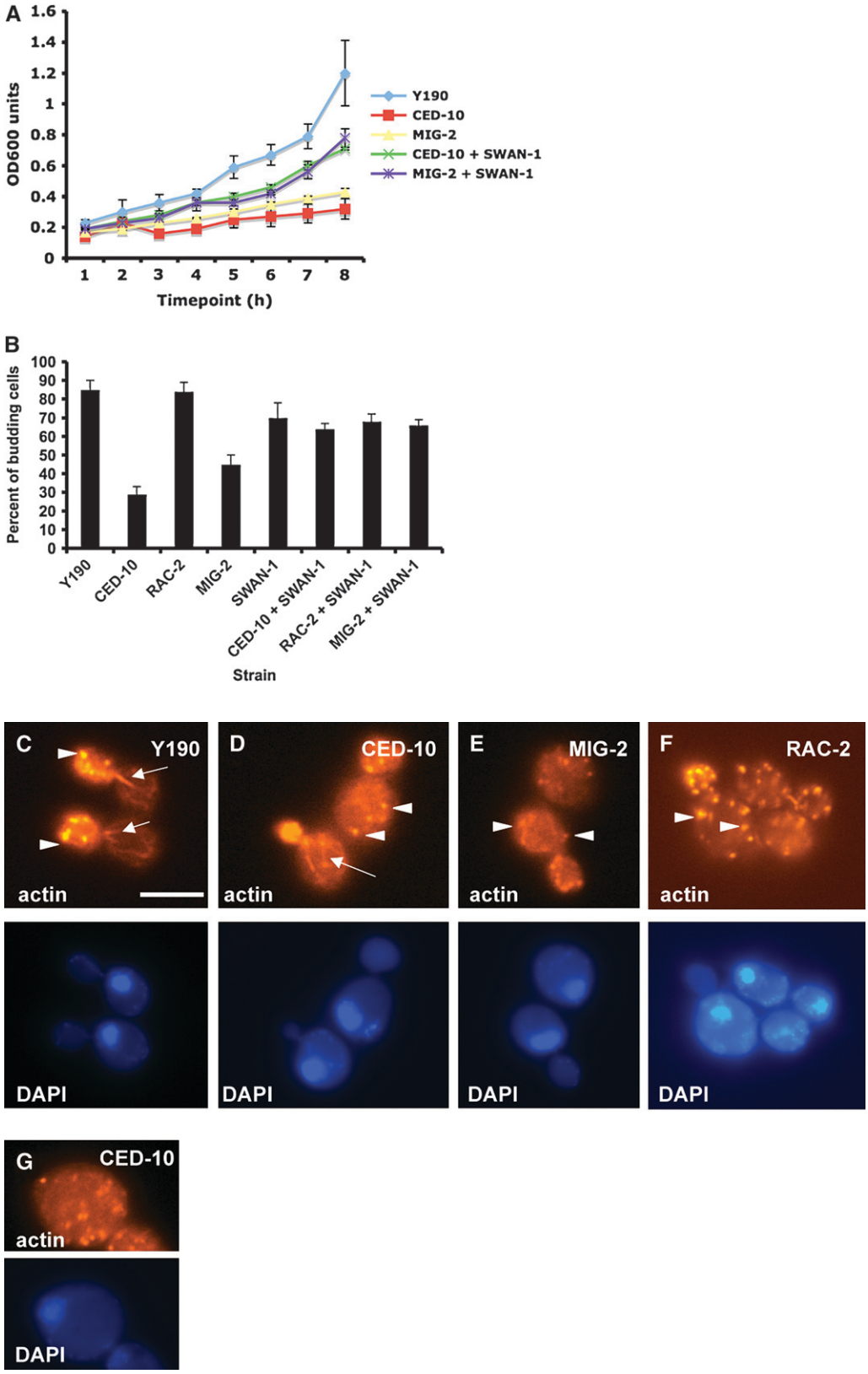

FIGURE 8.—SWAN-1 inhibits *C. elegans* Rac activity in yeast. (A) A growth curve for yeast harboring different combinations of transgenes (*x*-axis is time point; *y*-axis is OD_{600}) (see MATERIALS AND METHODS). Y190 is the background strain, CED-10 and MIG-2 are fusions of the molecules with the DNA-binding domain of GAL4 in the pAS1-CYH two-hybrid vector, and SWAN-1 is a fusion of the molecule to the activation domain of GAL4 in the pACT two-hybrid vector. Error bars represent the standard deviation of two experiments. (B) Rac expression in yeast perturbs polarized cell division. Six hours after dilution to 0.1 OD_{600}, yeast cells harboring different transgenes (*x*-axis) were fixed and stained with rhodamine–phalloidin and DAPI. On the *y*-axis is the percentage of cells from each strain in the process of polarized cell budding. Error bars represent standard error of the proportion. (C–G) Fluorescence micrographs of yeast cells from different strains stained with rhodamine–phalloidin to visualize actin (actin) and DAPI to visualize DNA in the nucleus (DAPI). (C) Arrows point to polarized actin cables in the mother cell and arrowheads indicate the actin patches in the daughter cell. (D) The arrow points to a disorganized actin cable in a mother cell. (D–F) Arrowheads indicate actin patches ectopically present in mother cells. (G) A large, unpolarized cell undergoing nonpolarized growth without cell division. Bar in A, 10 μm.

and Cdc42p) (DONG *et al.* 2003). Several yeast Rho proteins are required to assemble the long actin filaments, which when absent lead to polarity defects and actin patch disorganization; and Cdc42p is required for the proper orientation of the long actin filaments. While yeast have no true Rac-family GTPases, transgenic expression of CED-10 Rac, RAC-2 Rac, and MIG-2 Rac in yeast might ectopically interfere with the normal roles

of the yeast Rho GTPases, resulting in the cytoskeletal and cell polarity defects described above.

The growth defects caused by CED-10, RAC-2, and MIG-2 expression in yeast were reduced when the yeast were cotransformed with SWAN-1. Doubling time decreased in the SWAN-1 cotransformed strains (CED-10-expressing cells went from >10 to 4.5 hr, and MIG-2 cells went from 6 to 3.5 hr), and the percentages of budding cells increased (Figure 8A): 29% of CED-10-expressing cells were budding compared to 64% of CED-10 SWAN-1-expressing cells ($P < 0.001$). While the SWAN-1 cotransformed cells still showed some cytoskeletal disorganization, it was not as severe as that seen in CED-10 and MIG-2 alone, as indicated by increased percentages of budding cells. These data indicate that SWAN-1 repressed CED-10 and MIG-2 activity in yeast cells.

DISCUSSION

Previous studies indicate that the UNC-115/abLIM actin-binding protein controls lamellipodia and filopodia formation in response to Rac GTPase signaling (Struckhoff and Lundquist 2003; Yang and Lundquist 2005), but the details of this pathway, including other molecules involved, remain unclear. A two-hybrid screen with the UNC-115 LIM domains identified the novel SWAN-1 protein, the *C. elegans* member of a novel seven- or eight-WD-repeat protein family conserved in yeast, protozoa, plants, and animals. Subsequent directed two-hybrid tests and co-immunoprecipitation experiments revealed that SWAN-1 interacted both with the UNC-115 LIM domains and with each of the three *C. elegans* Rac-family GTPases CED-10, RAC-2, and MIG-2. SWAN-1 might represent a molecular link between Rac GTPases and UNC-115/abLIM. Functional assays in *C. elegans* neurons, cultured mammalian 3T3 fibroblasts, and yeast indicate that SWAN-1 is a new class of negative regulator of Rac GTPases.

Expression of activated Rac in *C. elegans* neurons leads to the formation of ectopic lamellipodia and filopodia that is partially dependent on UNC-115 (Struckhoff and Lundquist 2003). Loss of *swan-1* enhanced the effects of CED-10 and RAC-2 activity, and transgenic expression of wild-type *swan-1* repressed CED-10 and RAC-2 activity in neurons. In these transgenic assays, no effect of SWAN-1 on MIG-2 activity was detected, despite the fact that SWAN-1 and MIG-2 interacted strongly in the two-hybrid system. *swan-1* loss of function did enhance the effects of dominant *mig-2* alleles on axon pathfinding, suggesting that SWAN-1 also regulates MIG-2. SWAN-1 also repressed MIG-2 activity in yeast, consistent with the idea that SWAN-1 regulates all three Racs, CED-10, RAC-2, and MIG-2. Expression of *C. elegans* SWAN-1 also suppressed the lamellipodia formed in 3T3 fibroblasts in response to human Rac1 harboring the activating Q61L mutation, suggesting that the Rac–SWAN-1 interaction has been conserved in the evolutionary divergence of humans and *C. elegans*.

swan-1 mutation also suppressed the cell corpse engulfment defects and gonadal distal tip cell migration defects of the hypomorphic *ced-10(n1993)* allele, indicating that SWAN-1 represses CED-10 activity in multiple developmental processes. *swan-1* did not suppress the distal tip cell migration defects of *mig-2(mu28)*, which is a predicted null allele of *mig-2*. *ced-10(n1993)* retains some *ced-10* activity, and this residual activity might be enhanced by loss of *swan-1*. No residual MIG-2 activity is predicted to be present in the null *mig-2(mu28)* mutant.

These experiments in *C. elegans*, mammalian fibroblasts, and yeast support the idea that SWAN-1 inhibits Rac activity. *swan-1* mutants have no detectable phenotype on their own, and the effects of *swan-1* in *rac* mutant strains are generally weak albeit consistent across many different assays. Generally, sensitized backgrounds were required to see an effect of *swan-1* (*e.g.*, hypomorphic and dominant mutations in *rac* genes and transgenic expression assays). SWAN-1 inhibited human Rac1 and to a lesser extent MYR::UNC-115 in fibroblasts. Possibly SWAN-1 is a direct inhibitor of UNC-115. However, no effect of *swan-1* on *myr::unc-115* activity in *C. elegans* neurons was detected, and SWAN-1 inhibited Rac activity in the yeast *Saccharomyces cerevisiae*, which has no molecule similar to UNC-115 encoded in its genome (Goffeau *et al.* 1996). These data indicate that SWAN-1 is a direct inhibitor of Rac GTPase activity. The inhibition of MYR::UNC-115 by SWAN-1 in fibroblasts might be an indirect effect of Rac1 inhibition (*i.e.*, MYR::UNC-115 might still require Rac activity for full effect). However, it is possible that SWAN-1 is a direct inhibitor of both Rac and MYR::UNC-115.

The effects of SWAN-1 on Rac activity are weak. The related SWAN-2 molecule showed no detectable functional overlap or similarity to SWAN-1, suggesting that the two molecules have distinct functions. SWAN-1 might be a fine-scale modulator that is involved in precisely tuning the amount of Rac activity. Modest changes in the levels of Rac activity can have distinct physiological outcomes. For example, in *C. elegans*, reducing the copy number of *rac* genes can change an attractive semaphorin signal into a repulsive signal (Dalpe *et al.* 2004). In cultured mammalian fibroblasts, reduction of Rac1 activity by as little as 30% leads to a switch from random peripheral lamellipodia protrusion to directed protrusion and directed cell migration (Pankov *et al.* 2005). *rac* genes display redundant functions in *C. elegans* and Drosophila whereby progressive loss of *rac* gene activity leads to progressively more severe axon defects (Lundquist *et al.* 2001; Ng *et al.* 2002). While there is clear overlap in *rac* gene function, it is also possible that different levels of *rac* activity have distinct physiological effects on axon development. SWAN-1 could also be a Rac "fidelity

factor" ensuring that background or transient Rac activation is suppressed so that only strong, persistent Rac activity leads to directed protrusion. *swan-1(ok267)* has no detectable phenotype on its own, but it is possible that a subtle phenotype was not revealed in our endpoint phenotypic analysis (*e.g.*, the growth cones of *swan-1* animals might behave differently from those of wild type, but they might eventually reach their targets).

GTPase-activating proteins and guanine nucleotide dissociation inhibitors are a well-characterized family of Rac negative regulators. GAPs inhibit small GTPases by activating the GTPase activity of the molecules, favoring the inactive, GDP-bound state, and GDIs prevent GTPase interaction with the plasma membrane (Van Aelst and D'Souza-Schorey 1997; Michaelson *et al.* 2001). SWAN-1 does not resemble any known GAPs or GDIs, and, as expected, SWAN-1 does not act as a GAP on human Rac1 (I. Blasutig and A. Pawson, personal communication). SWAN-1 interacted physically with both wild-type and G12V-mutant-activated Rac molecules, and *swan-1* interacted genetically with a variety of *rac* dominant mutations, including the activating G12V and Q61L mutations and the dominant mutations *ced-10(n3246)*, *ced-10(n1993lq20)*, and *mig-2(lq13)*, which affect Rac by unknown mechanisms. SWAN-1 might bind to Racs and lock them in an inactive conformation, SWAN-1 might block sites of interaction with Rac effectors regardless of the GTP-bound state of Rac, or SWAN-1 might regulate Rac interaction with the plasma membrane.

UNC-115/abLIM and Racs act in the same pathway to promote protrusive activity. SWAN-1 was isolated by its ability to interact with UNC-115 LIM domains, and SWAN-1 is a negative regulator of Rac GTPases in the pathway. UNC-115/abLIM might act as a scaffold for a complex that includes both activators and inhibitors of protrusive activity. SWAN-1 might be recruited with the Rac effector UNC-115/abLIM to Racs to precisely control levels of Rac activity or to prevent spurious, transient Rac activity so that directed protrusion can occur.

We thank E. Struckhoff for technical assistance; R. Barstead, G. Molder, and the *C. elegans* Gene Knockout Consortium for *C. elegans* strains; R. Barstead for providing the two-hybrid cDNA library; T. Meyer for providing the Rac1(Q61L) clone; K. Neufeld and T. C. Gamblin for reagents and technical assistance; and the Caenorhabditis Genetics Center, sponsored by the National Center for Research Resources, for providing *C. elegans* strains. This work was supported by National Institutes of Health (NIH) grant NS40945 and National Science Foundation grant IBN93192 to E.A.L. and NIH grant P20 RR016475 from the INBRE Program of the National Center for Research Resources.

LITERATURE CITED

Adams, A. E., and J. R. Pringle, 1984 Relationship of actin and tubulin distribution to bud growth in wild-type and morphogenetic-mutant Saccharomyces cerevisiae. J. Cell Biol. **98:** 934–945.

Dalpe, G., L. W. Zhang, H. Zheng and J. G. Culotti, 2004 Conversion of cell movement responses to Semaphorin-1 and Plexin-1 from attraction to repulsion by lowered levels of specific RAC GTPases in C. elegans. Development **131:** 2073–2088.

de Vetten, N., F. Quattrocchio, J. Mol and R. Koes, 1997 The *an11* locus controlling flower pigmentation in petunia encodes a novel WD-repeat protein conserved in yeast, plants and animals. Genes Dev. **11:** 1422–1434.

Dickson, B. J., 2001 Rho GTPases in growth cone guidance. Curr. Opin. Neurobiol. **11:** 103–110.

Dickson, B. J., 2002 Molecular mechanisms of axon guidance. Science **298:** 1959–1964.

Dong, Y., D. Pruyne and A. Bretscher, 2003 Formin-dependent actin assembly is regulated by distinct modes of Rho signaling in yeast. J. Cell Biol. **161:** 1081–1092.

Epstein, H. F., and D. C. Shakes, 1995 *Caenorhabditis elegans: Modern Biological Analysis of an Organism.* Academic Press, New York.

Goffeau, A., B. G. Barrell, H. Bussey, R. W. Davis, B. Dujon *et al.*, 1996 Life with 6000 genes. Science **274:** 546, 563–567.

Hall, A., 1998 Rho GTPases and the actin cytoskeleton. Science **279:** 509–514.

Kamath, R. S., and J. Ahringer, 2003 Genome-wide RNAi screening in Caenorhabditis elegans. Methods **30:** 313–321.

Kishore, R. S., and M. V. Sundaram, 2002 ced-10 Rac and mig-2 function redundantly and act with unc-73 trio to control the orientation of vulval cell divisions and migrations in Caenorhabditis elegans. Dev. Biol. **241:** 339–348.

Lundquist, E. A., 2003 Rac proteins and the control of axon development. Curr. Opin. Neurobiol. **13:** 384–390.

Lundquist, E. A., R. K. Herman, J. E. Shaw and C. I. Bargmann, 1998 UNC-115, a conserved protein with predicted LIM and actin-binding domains, mediates axon guidance in C. elegans. Neuron **21:** 385–392.

Lundquist, E. A., P. W. Reddien, E. Hartwieg, H. R. Horvitz and C. I. Bargmann, 2001 Three C. elegans Rac proteins and several alternative Rac regulators control axon guidance, cell migration and apoptotic cell phagocytosis. Development **128:** 4475–4488.

Michaelson, D., J. Silletti, G. Murphy, P. D'Eustachio, M. Rush *et al.*, 2001 Differential localization of Rho GTPases in live cells: regulation by hypervariable regions and RhoGDI binding. J. Cell Biol. **152:** 111–126.

Neer, E. J., C. J. Schmidt, R. Nambudripad and T. F. Smith, 1994 The ancient regulatory-protein family of WD-repeat proteins. Nature **371:** 297–300.

Ng, J., T. Nardine, M. Harms, J. Tzu, A. Goldstein *et al.*, 2002 Rac GTPases control axon growth, guidance and branching. Nature **416:** 442–447.

Otieno, C. J., J. Bastiaansen, A. M. Ramos and M. F. Rothschild, 2005 Mapping and association studies of diabetes related genes in the pig. Anim. Genet. **36:** 36–42.

Pankov, R., Y. Endo, S. Even-Ram, M. Araki, K. Clark *et al.*, 2005 A Rac switch regulates random versus directionally persistent cell migration. J. Cell Biol. **170:** 793–802.

Raftopoulou, M., and A. Hall, 2004 Cell migration: Rho GTPases lead the way. Dev. Biol. **265:** 23–32.

Reddien, P. W., and H. R. Horvitz, 2000 CED-2/CrkII and CED-10/Rac control phagocytosis and cell migration in Caenorhabditis elegans. Nat. Cell Biol. **2:** 131–136.

Shakir, M. A., J. S. Gill and E. A. Lundquist, 2006 Interactions of UNC-34 Enabled with Rac GTPases and the NIK kinase MIG-15 in *Caenorhabditis elegans* axon pathfinding and neuronal migration. Genetics **172:** 893–913.

Smith, T. F., C. Gaitatzes, K. Saxena and E. J. Neer, 1999 The WD repeat: a common architecture for diverse functions. Trends Biochem. Sci. **24:** 181–185.

Sondek, J., A. Bohm, D. G. Lambright, H. E. Hamm and P. B. Sigler, 1996 Crystal structure of a G-protein beta gamma dimer at 2.1A resolution. Nature **379:** 369–374.

Soto, M. C., H. Qadota, K. Kasuya, M. Inoue, D. Tsuboi *et al.*, 2002 The GEX-2 and GEX-3 proteins are required for tissue morphogenesis and cell migrations in C. elegans. Genes Dev. **16:** 620–632.

Steven, R., T. J. Kubiseski, H. Zheng, S. Kulkarni, J. Mancillas *et al.*, 1998 UNC-73 activates the Rac GTPase and is required for cell and growth cone migrations in *C. elegans*. Cell **92:** 785–795.

Struckhoff, E. C., and E. A. Lundquist, 2003 The actin-binding protein UNC-115 is an effector of Rac signaling during axon pathfinding in C. elegans. Development **130:** 693–704.

Tessier-Lavigne, M., and C. S. Goodman, 1996 The molecular biology of axon guidance. Science **274:** 1123–1133.

Timmons, L., D. L. Court and A. Fire, 2001 Ingestion of bacterially expressed dsRNAs can produce specific and potent genetic interference in Caenorhabditis elegans. Gene **263:** 103–112.

Van Aelst, L., and C. D'Souza-Schorey, 1997 Rho GTPases and signaling networks. Genes Dev. **11:** 2295–2322.

Vicente-Manzanares, M., D. J. Webb and A. R. Horwitz, 2005 Cell migration at a glance. J. Cell Sci. **118:** 4917–4919.

Walker, A. R., P. A. Davison, A. C. Bolognesi-Winfield, C. M. James, N. Srinivasan *et al.*, 1999 The TRANSPARENT TESTA GLABRA1 locus, which regulates trichome differentiation and anthocyanin biosynthesis in Arabidopsis, encodes a WD40 repeat protein. Plant Cell **11:** 1337–1350.

White, J. G., E. Southgate, J. N. Thomson and S. Brenner, 1986 The structure of the nervous system of the nematode *Caenorhabditis elegans*. Philos. Trans. R. Soc. Lond. **314:** 1–340.

Yang, Y., and E. A. Lundquist, 2005 The actin-binding protein UNC-115/abLIM controls formation of lamellipodia and filopodia and neuronal morphogenesis in Caenorhabditis elegans. Mol. Cell. Biol. **25:** 5158–5170.

Yu, T. W., and C. I. Bargmann, 2001 Dynamic regulation of axon guidance. Nat. Neurosci. **4**(Suppl.): 1169–1176.

Zipkin, I. D., R. M. Kindt and C. J. Kenyon, 1997 Role of a new Rho family member in cell migration and axon guidance in C. elegans. Cell **90:** 883–894.

Communicating editor: D. I. Greenstein